4318 *Biochemistry* **2010,** *49,* 4318–4326
DOI: 10.1021/bi100118k

BIOCHEMISTRY
including biophysical chemistry & molecular biology
Article

Importance of the C-Terminal Loop L137−S141 for the Folding and Folding Stability of Staphylococcal Nuclease[†,‡]

Min Wang, Yingang Feng, Hongwei Yao, and Jinfeng Wang*

National Laboratory of Biomacromolecules, Institute of Biophysics, Chinese Academy of Sciences, 15 Datun Road, Beijing 100101, China

Received January 26, 2010; Revised Manuscript Received April 22, 2010

ABSTRACT: The role of the C-terminal loop L137−S141 in the folding and folding stability of staphylococcal nuclease (SNase) was investigated by deletion mutation. The C-terminal truncated SNase fragments, SNase137, SNase139, SNase140, and SNase141 containing residues 1−137, 1−139, 1−140, and 1−141, respectively, were adopted in this study. Folding states of these four SNase fragments were analyzed by circular dichroism and fluorescence measurements. The solution structure of SNase140 was determined and compared to those of SNase141 and native SNase using the heteronuclear NMR method. The results showed that folding of the four SNase fragments is correlated with the folding of helix α3. With the chain length extending from L137 and I139 to S141, folding of the fragments progressively approached to the tertiary folding of native SNase, and the folding stability was enhanced. These observations revealed that the C-terminal loop L137−S141 has profound effect not only on the folding of helix α3 but also on the stabilizing folding of both the α- and *β*-subdomains of SNase. Analysis indicates that stabilizing folding of the SNase and SNase fragments depends to a large extent on the hydrophobic packing interactions in both the C-terminal local structural region surrounding W140 including the loop L137−S141 and the N-terminal local structural region of the "*β*-barrel" hydrophobic core.

Over the past years, a number of studies have been carried out on addressing the information necessary for stabilizing the folding of staphylococcal nuclease (SNase)[1] encoded by the protein sequence (*1*−*6*). SNase is a widely used model system for the study of protein folding, which is composed of two subdomains, a large N-terminal *β*-subdomain and a small C-terminal α-subdomain. The N-terminal *β*-subdomain is constructed by a "*β*-barrel" core and two helices α1 (A58−A69) and α2 (V99−Q106) as well as the p-loop (pdTp-binding loop, D77−L89) and Ω-loop (P42−P56), whereas the C-terminal α-subdomain contains mainly a helix α3 (E122−K136) and the subsequent helical turn L137−S141 and the N- and C-terminal loops of the subdomain (*7*, *8*). A mixture of the N-terminal *β*-subdomain fragment and the C-terminal α-subdomain fragment can form a noncovalent complex through a folding-on-binding event, which generates a tertiary structure nearly identical to the structure of native SNase. For this, the crucial elements in the surface region of the binding interface between two subdomains are required, which establish the interactions necessary for stabilizing the native-like folding of both fragments (*8*). The C-terminal amino acids 137−149 of SNase were proposed to contain critical information for the native folding of SNase (*1*, *2*). The 3D solution structure of full-length SNase shows that the loop L137−S141 connecting to the C-terminal end of the helix α3 has a helical-turn conformation (*7*). W140 in this loop region is a key residue which bears information important to both long-range and short-range interactions for the structure and stability of SNase and plays an important role in maintaining protein tertiary integrity (*3*−*6*). The side chain of the residue at position 140 is required to be tryptophan; however, the backbone of 141th residue is solely critical for foldability, but the side chain information is not crucial (*1*, *2*, *6*).

To advance investigations into the importance of the loop L137−S141 in the folding of SNase, we have expressed and purified the C-terminal truncated SNase fragments retaining an integral sequence of the helix α3: SNase137, SNase139, SNase140, and SNase141 containing residues 1−137, 1−139, 1−140, and 1−141, respectively. The folding states of these fragments were analyzed by circular dichroism (CD) and fluorescence measurements. The solution structure of SNase140 was determined, and the backbone internal motions of SNase140 were compared to those of SNase141 and native SNase using the heteronuclear NMR method. Roles of the C-terminal loop L137−S141 in the folding of helix α3 and in stabilizing the folding of two subdomains of SNase are described in detail.

MATERIALS AND METHODS

Protein Expression and Purification. Four SNase fragments, namely, SNase137, SNase139, SNase140, and SNase141 containing residues 1−137, 1−139, 1−140, and 1−141, respectively, were expressed and purified for the present study. The expression plasmids containing the genes of these four C-terminal

[†]This research was supported by the National Natural Science Foundation of China (NNSFC), 30570375, and partially by the NNSFC, 39823001.

[‡]The atomic coordinates and NMR restraints of SNase140 have been deposited in the Protein Databank under ID code 2kq3. The chemical shifts of SNase140 have been deposited in the BioMagResBank database with accession number 16585.

*To whom correspondence should be addressed. Tel: +86 10 64888490. Fax: +86 10 64872026. E-mail: jfw@sun5.ibp.ac.cn.

[1]Abbreviations: SNase, staphylococcal nuclease; pdTp, thymidine 3′,5′-bisphosphate; CD, circular dichroism; TMAO, trimethylamine *N*-oxide; DSS, 2,2-dimethyl-2-silapentane-5-sulfonate.

 Published on Web 04/23/2010

truncated SNase fragments were obtained by site-directed mutagenesis using pET3a-SNase as template and were sequenced to confirm the presence of the desired mutations. The plasmids were then transferred into the BL21(DE3)/pLysS strain of *Escherichia coli*.

All four C-terminal truncated SNase fragments and native SNase were overexpressed and purified according to the procedures described previously (*9*). Uniformly ^{15}N- and/or ^{13}C-labeled SNase fragments for NMR studies were obtained through bacterial growth in M9 minimal medium containing $^{15}NH_4Cl$ and/or [^{13}C]glucose as the sole nitrogen and/or carbon sources, respectively. The purity of proteins was checked by SDS−PAGE to ensure a single band.

CD Measurements. Far-UV CD (200−250 nm) spectra were recorded for SNase137, SNase139, SNase140, SNase141, and native SNase on a Jasco J-720 circular dichroism spectropolarimeter at 25 °C. A 1.0 mm cuvette path length was employed in the measurements. Four scans were averaged for each measurement. The sample used for recoding the CD spectra was 20 μM proteins in 20 mM Tris-HCl buffer (pH 7.4). The concentration of the purified protein was evaluated from the UV absorbance at 280 nm using the calculated extinction coefficient 14650 M^{-1} cm^{-1} for native SNase, SNase141, and SNase140 and 8960 M^{-1} cm^{-1} for SNase139 and SNase137.

For urea-denaturation measurements, the ellipticity at wavelength 222 nm of the far-UV CD spectrum was used to monitor the unfolding transitions of SNase137, SNase139, SNase140, SNase141, and native SNase. All measurements were performed with 30 μM SNase and SNase fragments dissolved in the buffer containing 20 mM Tris-HCl (pH 7.4) which were incubated overnight at 25 °C in the presence of various urea concentrations.

Fluorescence Measurements. The intrinsic tryptophan fluorescence emission spectra of SNase140, SNase141, and native SNase were recorded on a Hitachi F-4500 fluorescence spectrophotometer at 25 °C. Protein concentrations were 3 μM in a 20 mM Tris-HCl buffer, pH 7.4. All experiments were conducted with a 5 mm slit width by using 295 nm as the excitation wavelength. The emission spectra of tryptophan scanned from 300 to 400 nm were recorded.

Enzymatic Activity Assay. Enzymatic activity assay was achieved according to the method described by Cautrecasas et al. (*10*). The enzyme activities for hydrolysis of single-stranded DNA were measured for SNase137, SNase139, SNase140, SNase141, and full-length SNase. All measurements were performed at 25 °C with a Hitachi UV-2010 spectrophotometer by monitoring the increase in absorbance at 260 nm. One unit of the enzymatic activity is defined as the amount of enzyme causing a change of 1.0 absorbance unit/min at 260 nm in a 1.0 cm cell. The single-strand salmon sperm DNA, obtained by boiling salmon sperm DNA at 100 °C for 30 min and rapidly cooled on ice, was used as a substrate of measurements. The reaction mixture contained 50 μg/mL single-strand salmon sperm DNA, 20 mM Tris-HCl, and 10 mM $CaCl_2$, pH 7.4. The nuclease activity was evaluated by examining the initial slope of the absorbance change (the increment of OD_{260} at the first 60 s).

NMR Spectroscopy. NMR samples were prepared as follows: 1.0−2.0 mM ^{15}N- or ^{13}C/^{15}N-labeled protein in 90% H_2O/10% D_2O containing 50 mM deuterated acetate buffer (pH 5.0), 250 mM KCl, 1.0 mM EDTA, 0.02% NaN_3, and 0.2 mM DSS.

All heteronuclear NMR experiments (*11*) were run on a Bruker DMX600 spectrometer equipped with a *z*-gradient triple-resonance cryoprobe at 300 K. The 3D ^{1}H−^{13}C−^{15}N HNCA, HNCACB, CBCA(CO)NH, HBHA(CO)NH, (H)CC(CO)NH, HNCO, and 3D ^{1}H−^{15}N TOCSY-HSQC (τ_m = 80 ms), 3D ^{1}H−^{13}C HC(C)H−COSY and HC(C)H-TOCSY (τ_m = 12 ms) experiments were performed for backbone resonance assignments of SNase140 and native SNase and side chain resonance assignments of SNase140. NOE distance constraints of SNase140 were obtained by the 3D ^{1}H−^{15}N NOESY-HSQC and ^{1}H−^{13}C NOESY-HSQC experiments with mixing time τ_m = 120 and 130 ms, respectively. In estimation of hydrogen bond restraints, the slowly H/D exchange experiments were performed with SNase140. The 2D ^{1}H−^{15}N HSQC experiments were run for SNase140, SNase141, and native SNase and for SNase137 and SNase139 in the absence and presence of 2.0 M trimethylamine *N*-oxide (TMAO).

^{15}N relaxation parameters (T_1, T_2, and ^{1}H−^{15}N NOE) were measured for SNase140, SNase141, and native SNase at 300 K using the standard methods (*12*). For ^{15}N T_1 measurements, the delay times were set to 10×2, 60, 130, 220, 320, 440, 590, 780, 980, 1230, 1500, and 1850 ms. For T_2 measurements, the relaxation delays were 17×2, 34, 51, 68, 85, 102, 119, 136, 153, 170, 187, 204, and 238 ms. In the 2D ^{1}H−^{15}N NOE experiments, a delay of 5 s was followed by ^{1}H saturation for 3 s, whereas the saturation period was replaced by a delay of 8 s in the control experiment. Two experiments were run in an interleaved manner.

All NMR data were processed and analyzed using FELIX software (Accelrys Inc.). ^{1}H chemical shifts were referenced to internal DSS. ^{15}N and ^{13}C chemical shifts were referenced indirectly (*13*).

Structure Calculation. Solution structures of SNase140 were calculated with the program CNS 1.1 (*14*). All assigned intramolecular NOEs for SNase140 were grouped into four classes of distance restraints with upper limits of 2.8, 3.7, 4.5, and 5.7 Å. The hydrogen bond restraints were determined according to the slowly exchanging amide protons and the predicted secondary structures using the CSI protocol. The backbone torsion angle restraints (φ and ψ) were derived from backbone chemical shifts using TALOS (*15*). A family of 100 structures was generated, from which a final set of the 20 structures of SNase140 with lowest energies was considered for use in the analysis of structural statistics. Structural analysis and statistics were obtained using the programs MOLMOL (*16*) and PROCHECK-NMR (*17*).

Determination of Unfolding Free Energy. For determination of the unfolding free energy of SNase137, SNase139, SNase140, SNase141, and native SNase, the unfolding curves were obtained by following the changes in ellipticity with varying urea concentrations between 0 and 6.0 M. The fraction of unfolded species (F_{unf}) was estimated according to the equation $F_{unf} = ([\theta] - [\theta]_N)/([\theta]_U - [\theta]_N)$, where N and U stand for the ellipticities of the folded and fully unfolded species, respectively. The F_{unf} values were calculated from the linear extrapolation of the pre- and postunfolding baselines. The unfolding free energy and m values in the relation $\Delta G = \Delta G°(H_2O) + m[D]$ were obtained by fitting the denaturation data to a two-state model using the standard equation (*18*, *19*).

Determination of Backbone Dynamic Parameters. Analyses of ^{15}N relaxation parameters of backbone internal motions were performed following the methods described previously (*20*, *21*). R_1 and R_2 relaxation rates for each residue were determined by fitting peak intensities of the spectra acquired at various relaxation delay times to an exponential decay function, $I/I_0 = \exp(-R_{1,2}t)$, where I_0 is the intensity at $t = 0$ and I is the

intensity after a time delay t. The steady-state $^1H-^{15}N$ NOEs were calculated from the ratio of peak intensities in the NOE spectra obtained with and without proton presaturation. R_2/R_1 ratios of a set of residues selected by excluding residues with very high R_2 and low NOE values (<0.65) were used to initially estimate the rotational correlation time (τ_m). Analysis of the rotational diffusion tensor was performed using the program TENSOR 2.0 (*22*). The optimized overall tumbling correlation time of the molecule (τ_m) was obtained as 9.23, 9.62, and 9.95 ns, and the axial symmetric diffusion tensor components $D_{\|}/D_{\perp}$ were 1.13, 1.19, and 1.17 for SNase140, SNase141, and native SNase, respectively. The axial symmetric model-free spectral density function was chosen to derive the dynamic parameters for the proteins. The N−H bond length was assumed to be 1.02 Å, and the N−H chemical shift anisotropy was taken as −160 ppm. A Lipari−Szabo analysis (*23*, *24*) was performed for all individual residues. Five model-free parameter sets were iteratively tested and selected as described by Mandel et al. (*25*). The confidence levels were estimated using 300 Monte Carlo simulations per run in combination with χ^2 and F-test criterion.

Table 1: Nuclease Activities Determined for the Four C-Terminal Truncated SNase Fragments and Full-Length SNase[a]

proteins	specific activity (units/mg)	relative activity
SNase	2553	1
SNase141	2298 ± 127	0.90 ± 0.05
SNase140	2018 ± 153	0.79 ± 0.06
SNase139	1319 ± 178	0.51 ± 0.07
SNase137	1270 ± 156	0.50 ± 0.06

[a]Relative activity = (specific activity of a given protein)/(specific activity of SNase).

RESULTS

Enzyme Activities of the Four SNase Fragments. The enzyme activity for hydrolysis of single-stranded DNA was measured for SNase137, SNase139, SNase140, and SNase141 and for full-length SNase and listed in Table 1. SNase137 and SNase139 have almost the same reduced nuclease activity (~50%) relative to the activity of native SNase. The enzyme activity was dramatically increased by elongating the peptide chain of SNase139 from residue I139 to residue W140 and further increased by elongating the peptide chain up to S141. SNase140 and SNase141 each showed activity comparable to that of native SNase; that is, the nuclease activities of SNase140 and SNase141 were 79% and 90% of the native level, respectively. These

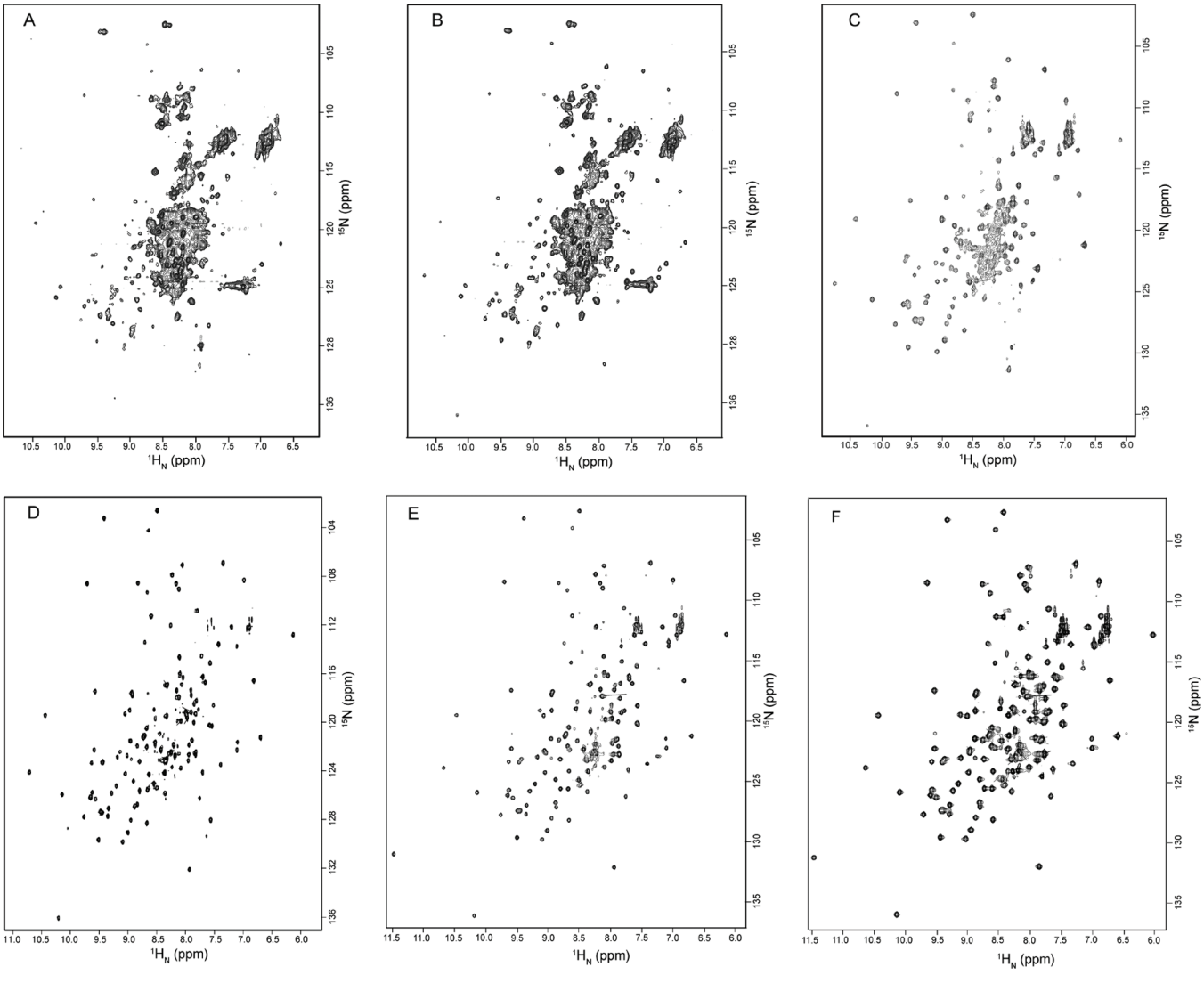

FIGURE 1: 2D $^1H-^{15}N$ HSQC spectra of the SNase fragments: SNase137 (A), SNase139 (B), SNase139 in the presence of 2.0 M TMAO (C), SNase140 (D), and SNase141 (E). The spectrum of native SNase (F) is provided for comparison.

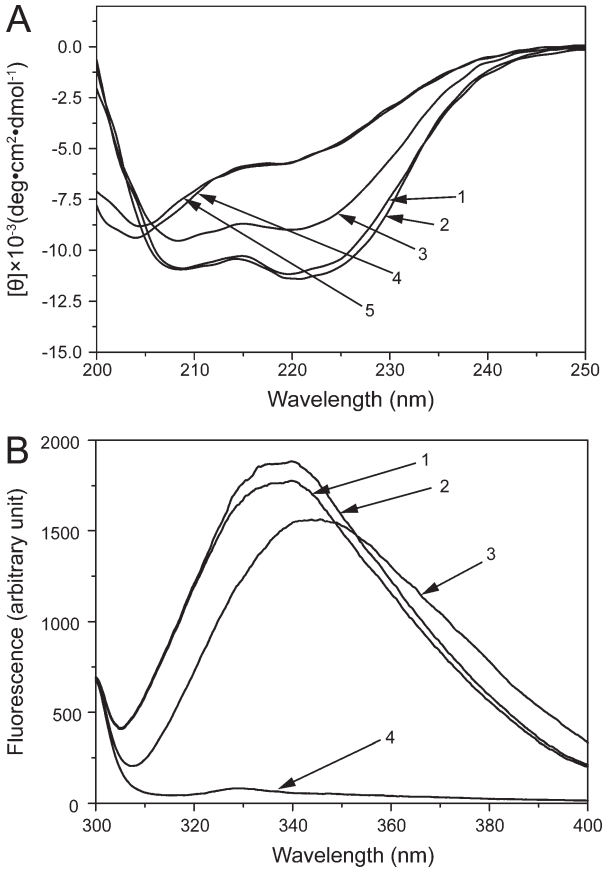

FIGURE 2: Far-UV CD spectra (A) and fluorescence spectra (B) of the SNase fragments in comparison with the spectrum of full-length SNase. Curves 1−5 denote the spectra of native SNase, SNase141, SNase140, SNase139, and SNase137, respectively.

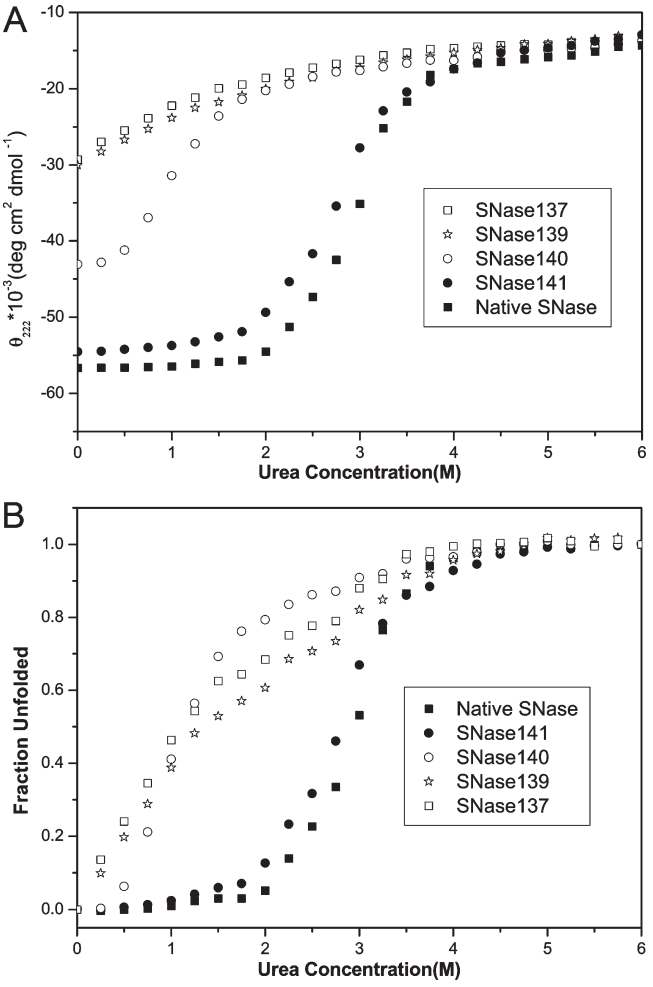

FIGURE 3: Urea-induced unfolding transitions monitored by far-UV CD at 222 nm for SNase137 (□), SNase139 (☆), SNase140 (○), and SNase141 (●). The unfolding transitions of native SNase (■) were also shown for comparison. (A) Plot of the molar ellipticity versus urea concentration. (B) Plot of the fraction unfolded as a function of urea concentration.

revealed that SNase140 and SNase141 must maintain the native-like conformation for ensuring a higher nuclease activity.

Folding Behaviors of the Four SNase Fragments. Folding of the four SNase fragments was detected using the 2D $^{1}H-^{15}N$ HSQC spectrum of the corresponding fragment. Figure 1 shows the 2D $^{1}H-^{15}N$ HSQC spectra of SNase137, SNase139, SNase140, and SNase141. The spectra of SNase137 and SNase139 (Figure 1A,B) provided a great number of cross-peaks squeezed into the narrow $^{1}H_N$ and ^{15}N chemical shift regions of 7.8−8.8 and 118−126 ppm, respectively. Moreover, these two spectra showed a number of relatively weak resonance peaks distributed in the 2D spectrum which is very similar to that in the spectrum of native SNase. Obviously, SNase137 and SNase139 were in the largely unfolded state which was in exchange with the partially folded state. However, the osmolyte force of 2.0 M TMAO can drive SNase137 and SNase139 to fold into a stable native-like structure. This is because the solvophobic effect of TMAO on the protein can make the unfolding state very unfavorable and can drive a native-like packing of hydrophobic residues (*26*). The 2D $^{1}H-^{15}N$ HSQC spectra of SNase137 (spectrum not shown) and SNase139 (Figure 1C) in the presence of 2.0 M TMAO showed distributed cross-peaks, and the distribution pattern of cross-peaks is similar to that observed in the spectrum of native SNase (Figure 1F). This implies the native-like folding of the helix α3 and the β-subdomain in the two fragments. Unlike SNase137 and SNase139, SNase140 and SNase141 provided 2D $^{1}H-^{15}N$ HSQC spectra (Figure 1D,E) which are about the same as the spectrum of native SNase (Figure 1F), showing well-dispersed cross-peaks in the whole spectral region. Therefore, SNase140 and SNase141 were in the native-like folded state.

The secondary structures of the four SNase fragments were detected by far-UV CD (Figure 2A). The CD spectra of SNase137 and SNase139 are largely different from that of native SNase as well as SNase141 and SNase140. Both spectra showed a pronounced negative signal at about 204 nm and a broad weak shoulder at 222 nm, which indicated that SNase137 and SNase139 were in a transient equilibrium involving species containing the partially folded and unfolded states in solution. The spectrum of SNase140 showed two negative minima at about 208 and 222 nm, reflecting a native-like conformation having ordered secondary structures. However, the ellipticity at 222 nm of SNase140 is lower than that of SNase141 and native SNase. The CD spectrum and the ellipticity at 222 nm of SNase141 are almost identical to those of native SNase. Therefore, SNase141 but not SNase140 demonstrated the same ordered secondary structures detected in native SNase.

Intrinsic tryptophan fluorescence spectra were also used to demonstrate the local structure of residue W140 in SNase140, SNase141, and native SNase since the intrinsic tryptophan fluorescence signal is sensitive to the changes in local environment of the tryptophan residue. Figure 2B shows that the

Table 2: Thermodynamic Parameters Derived from Urea-Induced Unfolding of SNase140 and SNase141 in Comparison with Those of Native SNase and SNase140 in the Presence of Calcium

proteins	$\Delta G°(H_2O)$ (kcal/mol)	m [kcal/(M·mol)]
SNase	6.0 ± 0.4	−2.1 ± 0.1
SNase141	4.9 ± 0.3	−1.8 ± 0.1
SNase140	1.1 ± 0.2	−1.6 ± 0.1
SNase140 + Ca^{2+}	2.6 ± 0.3	−2.3 ± 0.1

fluorescence spectra of SNase141 and native SNase are almost the same. However, the fluorescence intensity of SNase140 is decreased with a red shift in the fluorescence maximum as compared to that of SNase141 and native SNase. This indicated that residue W140 in SNase140 becomes less buried in the local structural region, and the conformation of the local environment of W140 in SNase140 is different from that of native SNase and SNase141.

The above results showed that the elongation of W140 after I139 changes dramatically the folding state of the SNase fragment, resulting in the formation of a native-like tertiary structure of SNase140. However, the conformation of the local structural region of residue W140 in SNase140 may be different from that in native SNase and SNase141.

Urea-Induced Denaturation of the Four SNase Fragments. Unfolding transitions of the four SNase fragments and native SNase were obtained by the far-UV CD measurement. Figure 3 shows the different denaturation curves for fragments SNase137, SNase139, SNase140, and SNase141. The unfolding of native SNase exhibited a two-state process as described previously (*27*). For SNase141, the unfolding curve showed a single and sharp sigmoidal profile which is very similar to the curve of native SNase. However, the nonsigmoidal denaturation curves were obtained for SNase137 and SNase139, revealing again that both of the fragments are represented as the ensembles of partially folded and unfolded species. Significant differences could be observed in the unfolding profile of SNase140. The unfolding curve of SNase140 barely reached a plateau at low urea concentrations and provided a lower midpoint of the transition (C_m, where 50% of the protein was unfolded), indicating that SNase140 unfolds easily compared to SNase141 and native SNase.

The apparent free energy for unfolding in the presence of urea ($\Delta G°(H_2O)$) and the slope of the transition (m) were calculated for SNase141 and native SNase (Table 2). The unfolding free energy of SNase141 is 4.9 ± 0.3 kcal/mol, which is lower than that of native SNase (6.0 ± 0.4 kcal/mol). For SNase140, the native baseline could not be well-defined according to Figure 3; nevertheless, the $\Delta G°(H_2O)$ and m values were estimated (even though the accuracy was limited) for comparative analysis. The estimated free energy of unfolding is ~1.1 ± 0.2 kcal/mol for SNase140 and 2.6 ± 0.3 kcal/mol for SNase140 in the presence of Ca^{2+}, which are much lower than that for native SNase and SNase141 (Table 2). Apparently, SNase140 has lower folding stability compared to native SNase and SNase141, whereas SNase137 and SNase139 have no capability to be in the fully folded state. The equilibrium behavior of SNase140 in the urea-induced unfolding process is quite different from that of native SNase and SNase141.

3D Solution Structure of SNase140. Solution structure of SNase140 was calculated using the intramolecular NOE-derived restraints in combination with the intramolecular dihedral angle

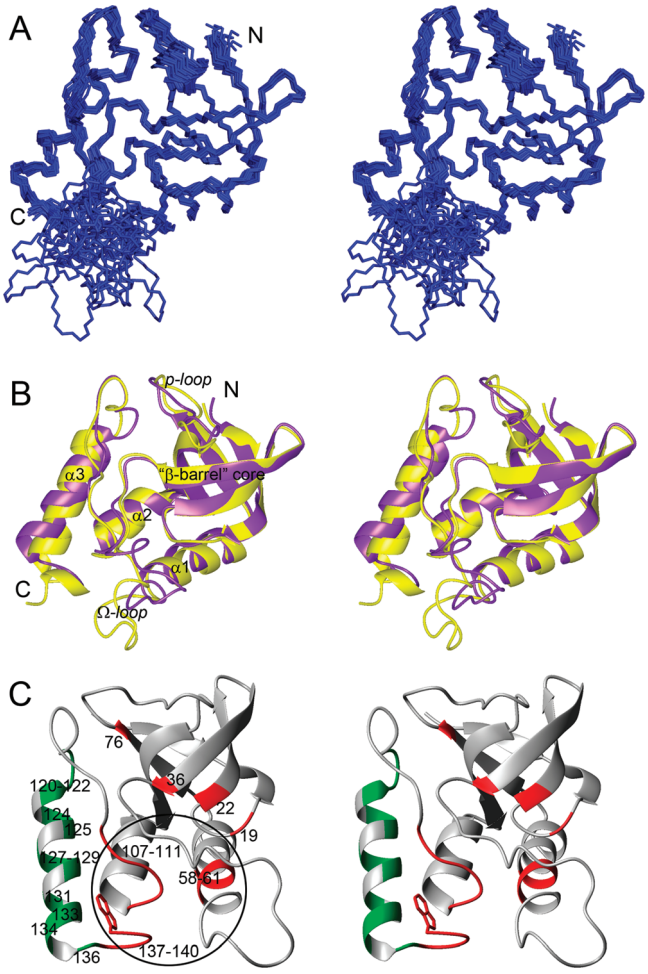

FIGURE 4: Solution structure of SNase140. (A) Superposition of the 20 lowest energy conformers calculated for SNase140. (B) Ribbon structure of a representative conformer of SNase140 (purple) superimposed to the structure of native SNase (yellow). (C) Mapping the residues showing relatively large NMR-derived chemical shift changes ($\Delta\delta_{comp} \geq 0.04$ ppm) on the structure of SNase140. The backbone tracings of these residues are colored in green (for residues mainly in helix α3) and red (for residues in the other regions). The large circle indicates the local structural region surrounding W140. Residues 1−7 of SNase140 and native SNase and the residues following 143 of native SNase are not shown.

and hydrogen bond restraints. The number of assigned NOEs and the distance restraints used in the structure calculations are summarized in Table S1 of the Supporting Information. An ensemble of the 20 lowest energy NMR-derived solution structures of SNase140 is shown in Figure 4A. The structural statistics of the SNase140 ensemble are summarized in Table S1 of the Supporting Information. The overall structure of SNase140 is essentially the same as that of native SNase (PDB code 1JOO) except for the C-terminal structural region of the protein (Figure 4B). In general, SNase140 has a folded native-like structure.

The structural deviations of SNase140 from native SNase were revealed by differences in the NMR-derived chemical shifts between two proteins. For SNase140, more than 95% and 90% of the backbone and side chain assignments were obtained, respectively. The assignments of amide resonances for SNase140 are shown in Figure S1 of the Supporting Information. The chemical shifts of $^1H_\alpha$, ^1H_N, and ^{15}N resonances for assigned residues of SNase140 were compared with that of native SNase (Figure S2 of the Supporting Information). Differences in the

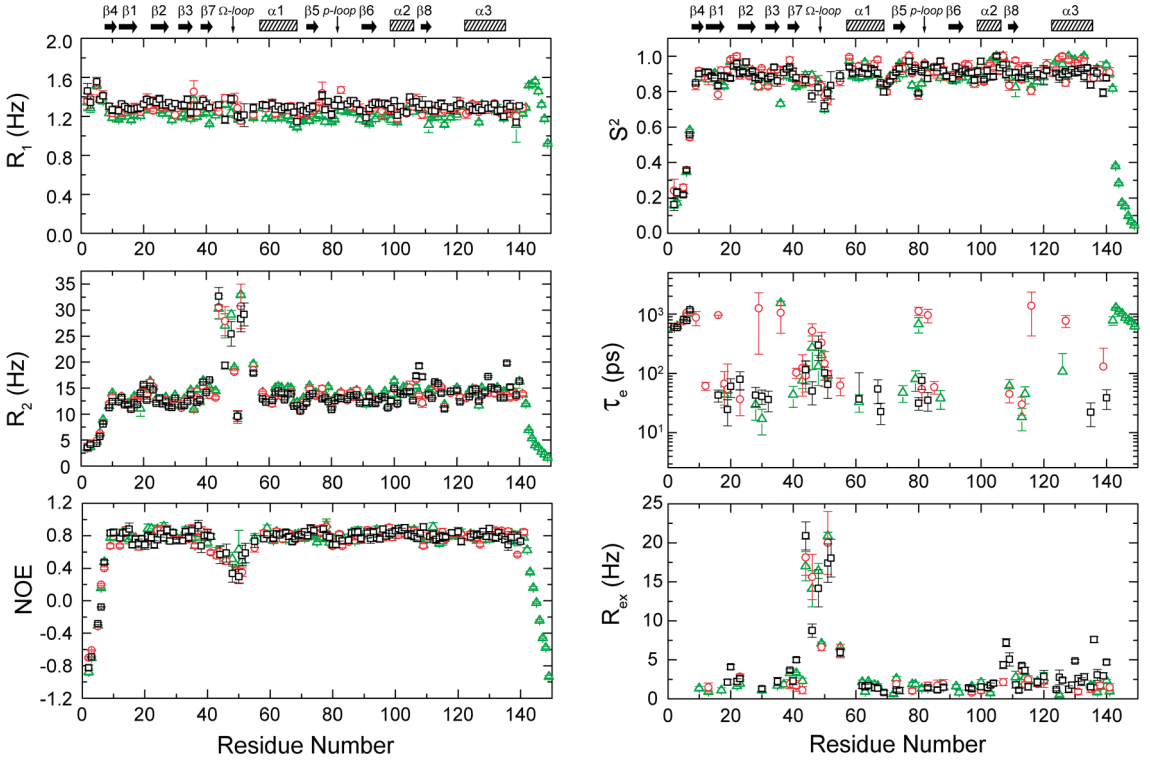

FIGURE 5: Sequence variation of ^{15}N relaxation parameters and model-free parameters of SNase140 (black) and SNase141 (red). The relaxation parameters of native SNase (green) are provided for comparison. Positions of the secondary structures are marked at the top of the diagrams.

chemical shifts, namely, $\Delta\delta = \delta(\text{SNase140}) - \delta(\text{SNase149})$, are small ($\Delta\delta H_\alpha$ and $\Delta\delta H_N < \pm 0.01$ ppm for > 58% of the assigned resonances; $\Delta\delta N < \pm 0.1$ ppm for > 64% of the assigned resonances). The relatively large weighted differences $\Delta\delta_{comp} = (\Delta\delta H_N^2 + 0.17\Delta\delta N^2)^{1/2}$ (> 0.05 ppm) can be observed for residues D40, T41, H46, K49, V51, and E52 in the Ω-loop; A60 in the N-terminal of helix α1; G107−A109 in the loop linking helix α2 and strand *β*8 (A109−V111); V111, T120, and H121 in the loop linking strand *β*8 and helix α3; L125, E129, K134, and K136 in the helix α3; and L137−W140 in the loop connecting to the C-terminal of helix α3. In these secondary structural regions, residues S59, A109, E129, K133, K136, and N138−W140 also have relatively large $\Delta\delta H_\alpha$ values (> ±0.05 ppm). As is shown in Figure 4C, the residues having relatively large chemical shift changes ($\Delta\delta_{comp} \geq 0.04$ ppm) are mainly localized in the two structural regions except the Ω-loop of the protein. The first is a local structural region surrounding W140 which includes the C-terminal loop L137−S141, loop G107−A109, and N-terminal portion of the helix α1. The second structural region includes the helix α3 and the C-terminal portion of loop A112−H121 which forms a DNA-binding cleft with the p-loop in the native SNase. It reflected that the structure of SNase140 in these regions should be deviated from that of native SNase.

Backbone Dynamics of SNase140, SNase141, and Native SNase. Relaxation parameters R_1, R_2, and ^{1}H−^{15}N NOEs of SNase140, SNase141, and native SNase are given in Figure 5. Sequence variations of these relaxation data are observed for the Ω-loop and for both N- and C-terminal regions of the proteins. The N-terminal regions of residues preceding E10 in SNase140 and SNase141 are flexible with ^{1}H−^{15}N NOE values < 0.6. Several detectable residues in the Ω-loop of SNase140 and SNase141 showed the ^{1}H−^{15}N NOE values < 0.4. All of the secondary structural regions except the Ω-loop and the terminal regions in SNase140 and SNase141 have ^{1}H−^{15}N NOE values similar to the values of native SNase (> 0.7), reflecting that the backbone high-frequency motions of these structural regions are highly restricted in both SNase140 and SNase141. The R_1 rates are fairly constant for SNase140, SNase141, and native SNase except the terminal regions, having the average values of 1.30 ± 0.03, 1.29 ± 0.3, and 1.22 ± 0.02, respectively. However, the R_2 rates for residues in the Ω-loop of SNase140, SNase141, and native SNase are higher than the average values of 14.04 ± 0.32, 13.82 ± 0.43, and 14.41 ± 0.27, respectively. In particular, certain residues of SNase140 such as G107−A109 linking the helix α2 and strand *β*8; Y113, V114, and T120 in the loop A112−H121; L125, R126, A130−K133, and K136 in the helix α3; and L137 and W140 in the C-terminal loop L137−W140 have R_2 rates explicitly higher than the average, indicating possible conformational exchange in these regions.

The model-free parameters S^2, τ_e, and R_{ex} obtained for SNase140, SNase141, and native SNase are shown in Figure 5. The average S^2 values for SNase140, SNase141, and native SNase except the Ω-loop and both terminal regions are 0.90 ± 0.02, 0.91 ± 0.02, and 0.89 ± 0.01, respectively, indicating the similar structural rigidity for these proteins. However, residues E122−W140 in SNase140, SNase141, and native SNase exhibited different amplitude of internal motions with average S^2 values of 0.89 ± 0.02, 0.93 ± 0.02, and 0.94 ± 0.01, respectively. This suggested that the helix α3 and C-terminal loop L137−W140 of SNase140 have relatively low motional restriction compared to SNase141 and native SNase, which may influence the backbone dynamic features of the segments in the close vicinity.

The R_{ex} contributions for the vast majority of the residues of SNase141 and native SNase except the residues in the Ω-loop are < 2.4 Hz (Figure 5), indicating that no explicit conformational exchange motions can be observed in the regular secondary structural regions of these proteins. However, residues G107−A109

linking the helix α2 and strand β8; Y113, V114, and T120 in the A112−H121 loop; L125, A130, Q131, K133, and K136 in the helix α3; and L137, I139, and W140 in the C-terminal loop L137-W140 of SNase140 display the large R_{ex} contributions in the range 2.6−7.6 Hz, indicating that the slow conformational exchange motions may occur to the corresponding structural regions.

Therefore, SNase141 and native SNase demonstrated approximately the same backbone internal motions except the C-terminal segment following residue S141 of native SNase. For SNase140, the backbone internal motions of the segment E10−Q106 are similar to those of SNase141 and native SNase. However, the A112−H121 loop and the C-terminal helix α3 and loop L137−W140 of SNase140 may undergo slow conformational exchange motions. Clearly, folding of SNase140 is less stable compared to SNase141 and native SNase.

DISCUSSION

Correlation of the Folding of Four SNase Fragments with the Folding of Helix α3. As is well-known, the equilibrium urea-denaturation experiments are often used to derive the free energy or *m*-value which is the criteria for determining protein stability. The four SNase fragments have different urea-induced denaturation curves provided by CD measurements (Figure 3), which probably associated with the folding state and folding stability of the helix α3.

In SNase141, an ordered helix α3 is well formed as demonstrated by X-ray crystal structure (*28*). The structure of SNase141 is almost identical to that of native SNase with rmsd of 0.1−0.4 Å by main chain superposition. The conformational difference was observed only in the segment K110−V114 of SNase141 having rmsd of 0.5−1.3 Å with native SNase. Especially, the main chain of Y113 in SNase141 is shifted and rotated toward the active site compared to native SNase, causing a spatial resistance for DNA binding (*28*), which may influence the enzyme activity of SNase141 compared to native SNase. From the structural description, it is reasonable that the thermal stability and backbone internal motions of SNase141 are very similar to those of native SNase.

The NMR-derived solution structure of SNase140 having a well-formed helix α3 is of striking resemblance to the tertiary structure of native SNase (Figure 4B). Nevertheless, the helix α3 of SNase140, especially the C-terminal region of helix α3, and the loop L137−W140 are located farther away from the main body structure. The backbone conformations of segment G107−A109 and segments around residues V111 and T120 are different from that of native SNase. Besides, the slow conformational exchange motions on the time scale of microseconds to milliseconds happened for the C-terminal region of helix α3 and loops G107−A109, A112−H121, and L137−W140 in SNase140. Clearly, the conformational change and conformational exchange motions of the backbone of helix α3 and loop L137−W140 at the C-terminal of SNase140 should affect the stability of SNase140. On the other hand, the possible slow conformational exchange motions of loop A112−H121 may cause some effect on enzyme activity of the protein since the certain degree of motional restriction of the A112−H121 loop, forming a putative DNA binding pocket with the p-loop, is one of the inherent features for SNase to exert enzyme function (*7*, *29*). In consequence, SNase140 exhibits the lower thermal stability and enzyme activity compared to SNase141 and native SNase.

Fragments SNase137 and SNase139 contain the complete sequence for helix α3. However, the stable ordered helix α3 was not formed in the two fragments as indicated by the CD spectra (Figure 2A), and both fragments were in the transient equilibrium between the partially folded and unfolded states in solution (Figure 2). Under the interaction of osmolyte TMAO, a native-like "β-barrel" hydrophobic core and the native-like hydrophobic packing between corresponding residues tend to form in the two fragments. This means the two fragments may lack the sufficient native-like tertiary interactions without the ordered helix α3.

As is analyzed above, evolution of the tertiary folding of the four SNase fragments is correlated with the evolution of formation of a stable ordered structure of the helix α3. As the chain lengths of the fragments progressively extend from L137 and I139 to S141, an ordered helix α3 is formed, and the tertiary folding and folding stability of the four SNase fragments are progressively approached to those of native SNase.

Implications for the Folding and Folding Stability of SNase. Both the previous and present studies of folding of SNase and its fragments indicate the importance of two structural regions for SNase in the stabilized fully folded state. The two structural regions include the "β-barrel" hydrophobic core consisting of six β-strands and the C-terminal local structural region surrounding W140 consisting of the C-terminal loop L137−S141, loop G107−A109, and the N-terminal portion of the helix α1.

(*A*) *Importance of the Integrate "β-Barrel" Hydrophobic Core for Folding of β-Subdomain*. Shortle's group has studied folding of a 131-residue SNase fragment (Δ131Δ-SNase) which was obtained by deleting residues 4−12 and 141−149 of the full-length SNase (*30*). In comparison with SNase140, Δ131Δ-SNase is a fragment shortening residues 4−12 which include residues K9−A12 forming the fourth β-strand in the "β-barrel" hydrophobic core of native SNase (*7*). According to the native SNase structure, deletion of one β-strand must disturb the main hydrophobic core of the protein (Figure 4B), perturbing the native-like hydrophobic packing interactions in the core and further destabilizing the N-terminal β-subdomain of the protein. Actually, in the folding of SNase, the "β-barrel" hydrophobic core as a large nonlocal nucleation site (*27*) or an individual cooperative folding unit (named as "foldon") (*31*, *32*) may form first and guide the subsequent folding of helices α1 (A58−A69) and α2 (V99−Q106) to progressively build the N-terminal β-subdomain, since the folding of helices α1 and α2 requires interactions with residues in the "β-barrel" core for stabilizing their helical conformations (*33*). This was demonstrated by the folding of G88W mutant 1−110 and 1−121 residue SNase fragments (SNase110 and SNase121). SNase110 and SNase121 are the fragments in the largely unfolded state. However, the G88W mutation intensifies the hydrophobic interactions in the "β-barrel" region and makes a well-packed, native-like "β-barrel" hydrophobic core in the two fragments, which drives the fragment folding to a native-like β-subdomain tertiary structure (*27*, *34*). Moreover, SNase140 containing an integrate "β-barrel" core structural region has a fully folded native-like structure. From these experimental facts, it is clear that disturbing the native hydrophobic core packing in the "β-barrel" structural region leads Δ131Δ-SNase to high unfolding under nondenaturing conditions as reported (*30*).

(*B*) *Importance of the C-Terminal Local Structural Region Surrounding W140 for Folding of Helix α3*. An early study on the peptide corresponding to residues E129−E142 of SNase has indicated that the presence of a helix between

residues E129 and K136 is consistent with the presence of a turn in the C-terminal region (L137−S141) (*35*). However, lacking the C-terminal loop L137−S141, the ordered helix α3 cannot be formed in the SNase fragments containing the complete sequence for helix α3, such as the fragments SNase139 and SNase137 in the present study and the fragment SNase136 including 1−136 residues of SNase in the previous study (*36*). Presumably, the C-terminal loop L137−S141 may have some inherent tertiary interactions with the helix, which contributes to the folding of helix α3. In native SNase, residues L137 and W140 in the loop L137−S141 are involved in the hydrophobic interactions with a long hydrophobic side chain ($C_{\beta-\xi}$) of an amphiphilic residue K133 in the helix α3 (*7*, *8*, *37*). Besides, the NH of L137 forms a hydrogen bond with CO of A132 (*37*). Referring to the description in the early report (*38*), L137 is a C-cap residue for the helix α3 of SNase, the hydrophobic contacts between K133 and W140 can be assigned to the hydrophobic contacts between a helical residue C4 and a residue C3′ in the subsequent loop, which could be regarded as hydrophobic C-capping interactions for the helix α3. The hydrophobic C-capping interactions can be enhanced by the hydrophobic interactions with C-cap residue L137. It seems the C-terminal loop L137−S141 may play a role of the C-terminal capping of helix α3 in SNase, since the loop L137−S141 has a helical-turn conformation for forming such hydrophobic C-capping interactions. In fact, the hydrophobic C-capping interactions for folding of helix α3 are a component part of the hydrophobic packing interactions of the pyrrole ring of W140 with the hydrophobic side chains of surrounding residues G107, L108, A109, and amphiphilic K110 from the *β*-subdomain and A132, L137, I139, and amphiphilic K133 from the α-subdomain (*7*, *37*), which serve as an anchoring force for specific association between the α- and *β*-subdomains of SNase (*8*). Together, these hydrophobic interactions make the local structural region surrounding W140 a small C-terminal hydrophobic core in native SNase. The hydrogen-bonding interactions between residues Y54OH−S141OG, G107O−I139N, L137O−W140N, and N138O−S141N (*7*, *37*) may also make contribution to producing the local structural order in this core region. Thus, the native local structure surrounding W140 constructed by the spatial pack of the loop L137−S141, loop G107−A109, and N-terminal portion of the helix α1 has key importance for the above-described tertiary interactions in the C-terminal of SNase. Apparently, changing the conformation of the local structure surrounding W140 including the helical-turn conformation of the loop L137−S141 will disturb the tertiary interactions in this local region, meanwhile influencing the stable folding of helix α3. This was evidenced by the folding state of the helix α3 in the four fragments. Unlike SNase141, the local structure surrounding W140 in SNase140 is different from that in native SNase (Figure 6), and the helix α3 may undergo the slow conformational exchange motion (Figure 5). For SNase137 and SNase139, lacking the native-like structure of this local region, a stable ordered helix α3 cannot be formed although they contain a full sequence of the helix α3.

(*C*) *The Hydrophobic Packing Interactions in These Two Structural Regions Dominate the Stabilized Folding of SNase*. As is analyzed above, SNase cannot be in the stabilized fully folded state if either the "*β*-barrel" hydrophobic core structure or the structure of the C-terminal local structural region surrounding W140 including the helical turn of the loop L137−S141 is disrupted. It is quite evident that any spatial structure changes in these two hydrophobic core regions can significantly disturb the hydrophobic packing interactions in these regions since the locally preexisting natural side chain packing arrangement may be destroyed in these regions. In SNase140, the chain truncation introduces a terminal carboxylic acid group for W140 that may not be compatible with its hydrophobic environments, which disturbs not only the conformation of the local structural region surrounding W140 but also the hydrophobic interactions in this local region. The intrinsic tryptophan fluorescence spectra of SNase140 (Figure 2B) provided evidence of the less burying W140 and the changes in conformation of the local environment of W140. This results in weakening the hydrophobic C-capping interactions for helix α3 and the anchoring interactions between two subdomains in SNase140. In consequence, the C-terminal α-subdomain cannot be stably packed on the N-terminal *β*-subdomain in SNase140. In SNase137 and SNase139, the C-terminal loop L137−S141 of helix α3 is destroyed. Thus, the hydrophobic C-capping interactions for helix α3 and the anchoring interactions between two subdomains in the local structural region surrounding W140 are disrupted, and the fragments lost the capability to fold into a native-like tertiary structure. In Δ131Δ-SNase, the segments for helices α1 and α2 have some residual helix structures, which is in the fast conformational averaging between helical and extended conformations. Besides, much less evidence for the residual helix structure was obtained for helix α3 (*26*). Obviously, the conformational changes must be happening with the N-terminal region of helix α1, the loop G107−A109 at the C-terminal of helix α2, and the subsequent loop L137−S141 of the helix α3 in Δ131Δ-SNase. In result, the tertiary interactions in the C-terminal local structural region surrounding W140 could be disrupted, and residue W140 in Δ131Δ-SNase cannot achieve such a role that is played in SNase140 for anchoring the C-terminal α-subdomain to the N-terminal *β*-subdomain. Therefore, Δ131Δ-SNase showed a totally different folding state compared to SNase140.

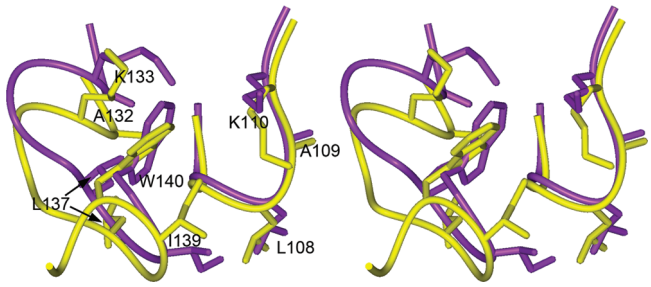

FIGURE 6: View on the side chain packing of the pyrrole ring of W140 in the hydrophobic environment formed by side chains of residues G107, L108, A109, A132, L137, and I139 and the long hydrophobic side chains ($C_{\beta-\xi}$) of amphiphilic residues K110 and K133 in SNase140 (purple) and native SNase (yellow).

Therefore, the results of the present study indicated that the inherent hydrophobic core packing in the "*β*-barrel" structural region and in the C-terminal local structural region surrounding W140 seems to dominate the folding and folding stability of SNase. The hydrophobic packing interactions in these two regions contribute specificity to SNase folding and stability in the native state. The loop L137−S141 having helical-turn conformation hasa profound effect not only on the folding of helix α3 but also on the stabilizing folding of both the α- and *β*-subdomains of SNase.

SUPPORTING INFORMATION AVAILABLE

Figures of residue-specific assignments for the backbone amide group of SNse140 and native SNase (Figure S1) and differences in the chemical shifts ($\Delta\delta$) of SNase140 from those of native SNase (Figure S2) and a table of experimental restraints and structural statistics for the families of 20 structures of SNase140. This material is available free of charge via the Internet at http://pubs.acs.org.

REFERENCES

1. Hirano, S., Kamikubo, H., Yamazaki, Y., and Kataoka, M. (2005) Elucidation of information encoded in tryptophan 140 of staphylococcal nuclease. *Proteins 58*, 271–277.
2. Hirano, S., Mihara, K., Yamazaki, Y., Kamikubo, H., Imamoto, Y., and Kataoka, M. (2002) Role of C-terminal region of staphylococcal nuclease for foldability, stability, and activity. *Proteins 49*, 255–265.
3. Shortle, D., and Meeker, A. K. (1986) Mutant forms of staphylococcal nuclease with altered patterns of guanidine hydrochloride and urea denaturation. *Proteins 1*, 81–89.
4. Calderon, R. O., Stolowich, N. J., Gerlt, J. A., and Sturtevant, J. M. (1985) Thermal-denaturation of staphylococcal nuclease. *Biochemistry 24*, 6044–6049.
5. Su, Z. D., Wu, J. M., Fang, H. J., Tsong, T. Y., and Chen, H. M. (2005) Local stability identification and the role of a key aromatic amino acid residue in staphylococcal nuclease refolding. *FEBS J. 272*, 3960–3966.
6. Yin, J. H., and Jing, G. Z. (2000) Tryptophan 140 is important, but serine 141 is essential for the formation of the integrated conformation of staphylococcal nuclease. *J. Biochem. 128*, 113–119.
7. Wang, J. F., Truckses, D. M., Abildgaard, F., Dzakula, Z., Zolnai, Z., and Markley, J. L. (1997) Solution structures of staphylococcal nuclease from multidimensional, multinuclear NMR: Nuclease-H124L and its ternary complex with Ca^{2+} and thymidine-3′,5′-bisphosphate. *J. Biomol. NMR 10*, 143–164.
8. Geng, Y., Feng, Y. G., Xie, T., Shan, L., and Wang, J. F. (2009) The native-like interactions between SNase121 and SNase(111−143) fragments induce the recovery of their native-like structures and the ability to degrade DNA. *Biochemistry 48*, 8692–8703.
9. Ye, K., Jing, G., and Wang, J. (2000) Interactions between subdomains in the partially folded state of staphylococcal nuclease. *Biochim. Biophys. Acta 1479*, 123–134.
10. Cuatrecasas, P., Fuchs, S., and Anfinsen, C. B. (1967) Catalytic properties and specificity of the extracellular nuclease of *Staphylococcus aureus*. *J. Biol. Chem. 242*, 1541–1547.
11. Sattler, M., Schleucher, J., and Griesinger, C. (1999) Heteronuclear multidimensional NMR experiments for the structure determination of proteins in solution employing pulsed field gradients. *Prog. Nucl. Magn. Reson. Spectrosc. 34*, 93–158.
12. Farrow, N. A., Muhandiram, R., Singer, A. U., Pascal, S. M., Kay, C. M., Gish, G., Shoelson, S. E., Pawson, T., Forman-Kay, J. D., and Kay, L. E. (1994) Backbone dynamics of a free and phosphopeptide-complexed Src homology 2 domain studied by ^{15}N NMR relaxation. *Biochemistry 33*, 5984–6003.
13. Markley, J. L., Bax, A., Arata, Y., Hilbers, C. W., Kaptein, R., Sykes, B. D., Wright, P. E., and Wuthrich, K. (1998) Recommendations for the presentation of NMR structures of proteins and nucleic acids (IUPAC Recommendations 1998). *Pure Appl. Chem. 70*, 117–142.
14. Brunger, A. T., Adams, P. D., Clore, G. M., DeLano, W. L., Gros, P., Grosse-Kunstleve, R. W., Jiang, J. S., Kuszewski, J., Nilges, M., Pannu, N. S., Read, R. J., Rice, L. M., Simonson, T., and Warren, G. L. (1998) Crystallography & NMR system: A new software suite for macromolecular structure determination. *Acta. Crystallogr., Sect. D: Biol. Crystallogr. 54*, 905–921.
15. Cornilescu, G., Delaglio, F., and Bax, A. (1999) Protein backbone angle restraints from searching a database for chemical shift and sequence homology. *J. Biomol. NMR 13*, 289–302.
16. Koradi, R., Billeter, M., and Wuthrich, K. (1996) MOLMOL: A program for display and analysis of macromolecular structures. *J. Mol. Graphics 14*, 51–55.
17. Laskowski, R. A., Rullmann, J. A. C., MacArthur, M. W., Kaptein, R., and Thornton, J. M. (1996) AQUA and PROCHECK-NMR: Programs for checking the quality of protein structures solved by NMR. *J. Biomol. NMR 8*, 477–486.
18. Pace, C. N. (1986) Determination and analysis of urea and guanidine hydrochloride denaturation curves. *Methods Enzymol. 131*, 266–280.
19. Santoro, M. M., and Bolen, D. W. (1988) Unfolding free energy changes determined by the linear extrapolation method. 1. Unfolding of phenylmethanesulfonyl alpha-chymotrypsin using different denaturants. *Biochemistry 27*, 8063–8068.
20. Viles, J. H., Duggan, B. M., Zaborowski, E., Schwarzinger, S., Huntley, J. J., Kroon, G. J., Dyson, H. J., and Wright, P. E. (2001) Potential bias in NMR relaxation data introduced by peak intensity analysis and curve fitting methods. *J. Biomol. NMR 21*, 1–9.
21. Hall, J. B., and Fushman, D. (2006) Variability of the ^{15}N chemical shielding tensors in the B3 domain of protein G from ^{15}N relaxation measurements at several fields. Implications for backbone order parameters. *J. Am. Chem. Soc. 128*, 7855–7870.
22. Dosset, P., Hus, J. C., Blackledge, M., and Marion, D. (2000) Efficient analysis of macromolecular rotational diffusion from heteronuclear relaxation data. *J. Biomol. NMR 16*, 23–28.
23. Lipari, G., and Szabo, A. (1982) Model-free approach to the interpretation of nuclear magnetic resonance relaxation in macromolecules. 1. Theory and range of validity. *J. Am. Chem. Soc. 104*, 4546–4559.
24. Lipari, G., and Szabo, A. (1982) Model-free approach to the interpretation of nuclear magnetic resonance relaxation in macromolecules. 2. Analysis of experimental results. *J. Am. Chem. Soc. 104*, 4559–4570.
25. Mandel, A. M., Akke, M., and Palmer, A. G., III (1995) Backbone dynamics of *Escherichia coli* ribonuclease HI: Correlations with structure and function in an active enzyme. *J. Mol. Biol. 246*, 144–163.
26. Baskakov, I., and Bolen, D. W. (1998) Forcing thermodynamically unfolded proteins to fold. *J. Biol. Chem. 273*, 4831–4834.
27. Xie, T., Liu, D., Feng, Y., Shan, L., and Wang, J. (2007) Folding stability and cooperativity of the three forms of 1−110 residues fragment of staphylococcal nuclease. *Biophys. J. 92*, 2090–2107.
28. Yang, Z., Ye, S., Jing, G. Z., Gui, L. L., and Liang, D. C. (1999) Crystal structure of an N-terminal fragment SNR141 of staphylococcal nuclease R refined at 1.9 Å resolution. *Prog. Nat. Sci. 9*, 617–622.
29. Shan, L., Tong, Y., Xie, T., Wang, M., and Wang, J. (2007) Restricted backbone conformational and motional flexibilities of loops containing peptidyl-proline bonds dominate the enzyme activity of staphylococcal nuclease. *Biochemistry 46*, 11504–11513.
30. Alexandrescu, A. T., Abeygunawardana, C., and Shortle, D. (1994) Structure and dynamics of a denatured 131-residue fragment of staphylococcal nuclease: Aa heteronuclear NMR study. *Biochemistry 33*, 1063–1072.
31. Maity, H., Maity, M., Krishna, M. M. G., Mayne, L., and Englander, S. W. (2005) Protein folding: The stepwise assembly of foldon units. *Proc. Natl. Acad. Sci. U.S.A. 102*, 4741–4746.
32. Lindberg, M. O., and Oliveberg, M. (2007) Malleability of protein folding pathways: A simple reason for complex behaviour. *Curr. Opin. Struct. Biol. 17*, 21–29.
33. Wang, M., Shan, L., and Wang, J. (2006) Two peptide fragments G55-I72 and K97-A109 from staphylococcal nuclease exhibit different behaviors in conformational preferences for helix formation. *Biopolymers 83*, 268–279.
34. Feng, Y., Liu, D., and Wang, J. (2003) Native-like partially folded conformations and folding process revealed in the N-terminal large fragments of staphylococcal nuclease: A study by NMR spectroscopy. *J. Mol. Biol. 330*, 821–837.
35. Maciejewski, M. W., and Zehfus, M. H. (1995) Structure of a compact peptide from staphylococcal nuclease determined by circular dichroism and NMR spectroscopy. *Biochemistry 34*, 5795–5800.
36. Flanagan, J. M., Kataoka, M., Shortle, D., and Engelman, D. M. (1992) Truncated staphylococcal nuclease is compact but disordered. *Proc. Natl. Acad. Sci. U.S.A. 89*, 748–752.
37. Hynes, T. R., and Fox, R. O. (1991) The crystal structure of staphylococcal nuclease refined at 1.7 Å resolution. *Proteins 10*, 92–105.
38. Ermolenko, D. N., Thomas, S. T., Aurora, R., Gronenborn, A. M., and Makhatadze, G. I. (2002) Hydrophobic interactions at the Ccap position of the C-capping motif of alpha-helices. *J. Mol. Biol. 322*, 123–135.